# Vacuum-Induced Wrinkle Arrays of InGaAs Semiconductor Nanomembranes on Polydimethylsiloxane Microwell Arrays

Doo-Seung Um,[†] Seongdong Lim,[†] Youngsu Lee,[†] Hochan Lee,[†] Hyung-jun Kim,[‡] Wen-Chun Yen,[§] Yu-Lun Chueh,[§] and Hyunhyub Ko[†,*]

[†]School of Energy and Chemical Engineering, Ulsan National Institute of Science and Technology (UNIST), Ulsan 689-798, Korea, [‡]Spin Convergence Research Center, Korea Institute of Science and Technology (KIST), Seoul 136-791, Korea, and [§]Department of Materials Science and Engineering, National Tsing Hua University, Hsinchu 30013, Taiwan, ROC

**ABSTRACT** Tunable surface morphology in III–V semiconductor nanomembranes provides opportunities to modulate electronic structures and light interactions of semiconductors. Here, we introduce a vacuum-induced wrinkling method for the formation of ordered wrinkles in InGaAs nanomembranes (thickness, 42 nm) on PDMS microwell arrays as a strategy for deterministic and multidirectional wrinkle engineering of semiconductor nanomembranes. In this approach, a vacuum-induced pressure difference between the outer and inner sides of the microwell patterns covered with nanomembranes leads to bulging of the nanomembranes at the predefined microwells, which, in turn, results in stretch-induced wrinkle formation of the nanomembranes between the microwells. The direction and geometry of the nanomembrane wrinkles are well controlled by varying the PDMS modulus, depth, and shape of microwells, and the temperature during the transfer printing of nanomembrane onto heterogeneous substrates. The wrinkling method shown here can be applied to other semiconductor nanomembranes and may create an important platform to realize unconventional electronic devices with tunable electronic properties.

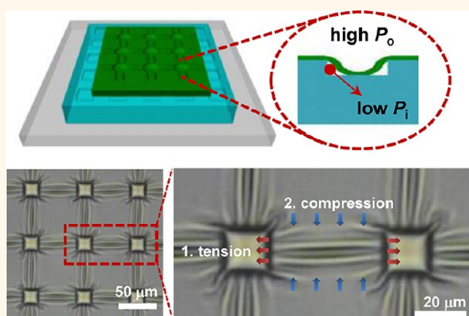


**KEYWORDS:** III–V semiconductor · InGaAs nanomembrane · vacuum-induced wrinkle · PDMS microwell · transfer printing

Heterogeneous integration of III–V compound semiconductor nanomembranes on arbitrary substrates provides great opportunities to fabricate high-performance electronic and optoelectronic devices on user-defined substrates (*i.e.*, Si, glass, polymers).[1] Recent advances in epitaxial transfer techniques, which are based on selective etching of sacrificial layers and transfer of active semiconductor layers using contact printing methods, have demonstrated high-mobility III–V semiconductor transistors,[2–4] metal-oxide-semiconductor field-effect-transistors (MOSFETs),[5,6] solar cells,[7] and light-emitting diodes (LEDs)[8,9] on silicon and plastic substrates. One of the advantages of epitaxial transfer techniques is tunable surface morphology and strain in the semiconductor nanomembranes during the transfer process, which provide new functionalities to improve device performance. For example, the accommodation of large strains in a structural configuration of wrinkled semiconductor films provides mechanical stretchability, enabling stretchable electronic devices.[10–14] The increase in active area and surface textures in semiconductor nanomembranes mediated by wrinkle formations have been utilized to improve light absorption, extraction, and scattering in organic and inorganic optoelectronic devices.[15–18] In addition to structural functionalities, the wrinkles in the semiconductor nanomembranes can induce compressive or tensile strains, which are known to significantly affect the electronic properties of the semiconductor and therefore the final device performance.[19–23] The wrinkle-induced periodic strain patterns in semiconductor nanowires or nanomembranes offer potential applications in single-element heterojunction superlattices,[24,25] photonic devices,[26] and thermoelectric devices.[27]

* Address correspondence to hyunhko@unist.ac.kr.

Received for review February 1, 2014 and accepted February 18, 2014.

Published online February 18, 2014
10.1021/nn500646j

© 2014 American Chemical Society

The general strategy of wrinkle formation is based on the application of a compressive stress on a stiff thin film sitting on top of a soft substrate, resulting in the development of surface wrinkles in the film that relax the applied compressive stress. Compressive stress has been applied in a number of different ways, for example, using thermal expansion/contraction,[28,29] solvent swelling/shrinkage,[30−33] and mechanical stretching/releasing to provide compressive strain.[10,34−36] These methods have been successfully applied for wrinkle engineering of polymers, metals, and semiconductor films. Although mechanical stretching/releasing methods have been successfully utilized for wrinkling of III−V nanoribbons,[11] these approaches only provide unidirectional wrinkles with the same wavelength and amplitude over the whole substrate area, which have a limitation in applications requiring deterministic and multidirectional wrinkles with different wavelengths and amplitudes. Patterning and ensuring deterministic locations of wrinkle arrays in inorganic semiconductor nanomembranes is still a great challenge in epitaxial lift-off and transfer of nanomembranes to arbitrary substrates.

Here, we present a vacuum-induced wrinkling method for deterministic and multidirectional wrinkle formation in InGaAs compound semiconductor nanomembranes on PDMS microwell arrays. The direction and geometry of the wrinkles can be easily controlled by the shape, location, depth, and alignment of the microwell arrays. Therefore, multidirectional and deterministic formation of various wrinkles with different wavelengths and amplitudes is achievable. Furthermore, we demonstrate epitaxial transfer of wrinkled InGaAs nanomembranes onto glass substrates and the controlled modulation of wrinkle wavelength and amplitude using thermal expansion/contraction of the PDMS microstamp during the transfer process.

## RESULTS AND DISCUSSION

Figure 1 shows a schematic illustration and the corresponding optical and scanning electron microscope (SEM) images of vacuum-induced wrinkle formation in the InGaAs semiconductor nanomembranes on a PDMS stamp with square-shaped microwell arrays (20 $\mu$m width, 1.2 $\mu$m height; the fabrication of PDMS stamp is shown in Supporting Information Figure S1). Briefly, the wrinkling process included the formation of InGaAs nanomembranes by selective wet-etching followed by vacuum-induced stretching of locally constrained InGaAs nanomembranes, resulting in the formation of wrinkle arrays in the predefined areas of the InGaAs nanomembranes. For fabrication of InGaAs nanomembranes on PDMS microwells, the epitaxially grown InAs/InGaAs/InAlAs stack layers on InP substrates (Supporting Information Figure S2) were attached to a PDMS stamp and etched in an HCl solution for selective wet-etching of the InP growth substrate and the InAlAs buffer layer. After the selective wet-etching process, the remaining InGaAs nanomembrane showed a vaguely square pattern that slightly followed the underlying microwell patterns of the PDMS stamp (Figure 1b,f). The areas between the microwell patterns showed a flat surface morphology. When a vacuum was applied to the chamber containing the samples, outward bulging of the nanomembranes occurred spontaneously (within several seconds) at the microwell patterned regions due to the sudden establishment of a pressure difference between the low $P_o$ (outer pressure) and high $P_i$ (inner pressure) across the nanomembranes on the microwell patterns ($P_o < P_i$, Figure 1c). This resulted in the formation of localized wrinkle arrays between the microwell patterns (Figure 1g, Supporting Information Video 1). Further application of the vacuum process for ~15 min induced air diffusion from the microwells to the outer regions through the PDMS and equilibrated $P_i$ and $P_o$ ($P_o = P_i$, Figure 1d), resulting in the depression of bulged nanomembranes and the subsequent disappearance of wrinkles (Figure 1h, Supporting Information Video 2). As a final step, when the vacuum was released, $P_o$ suddenly increases while $P_i$ remains at a lower pressure ($P_o > P_i$, Figure 1e), resulting in inward bulging of the nanomembranes and the subsequent formation of wrinkle arrays (Figure 1i, Supporting Information Video 3).

Vacuum-induced formation of wrinkles provided uniform and well-ordered arrays of wrinkles over a large area of nanomembranes (Figure 1j). The SEM image indicates that the nanomembranes were inwardly bulged into the PDMS microwells with wrinkle arrays between the microwells (Figure 1k). The wrinkle formation due to the bulging effects during the vacuum process can be explained by the following mechanism. The vacuum-induced nanomembrane bulging produces a longitudinal tension in the nanomembrane between the microwell patterns (Figure 1l). When the nanomembrane is stretched in one direction, it contracts in the other two perpendicular directions due to the Poisson effect. However, the two opposite boundaries are fixed to the microwell patterns and thus prevent Poisson contraction, which leads to the development of compressive stress in the transverse direction that can be relieved by nanomembrane wrinkling (Figure 1l). Similar wrinkling behavior was observed in a stretched, free-standing thin sheet clamped at two opposite ends, where the wrinkle formation was attributed to the instability of thin sheet that accommodated the compressive stress developed by constrained Poisson contraction near the fixed clamps.[37−39]

Vacuum-induced wrinkle formations on predefined microwell arrays allow deterministic formation of wrinkles with various geometries at predefined locations. As can be seen in Figure 2, different sizes and geometries of wrinkles can be fabricated using the vacuum-induced

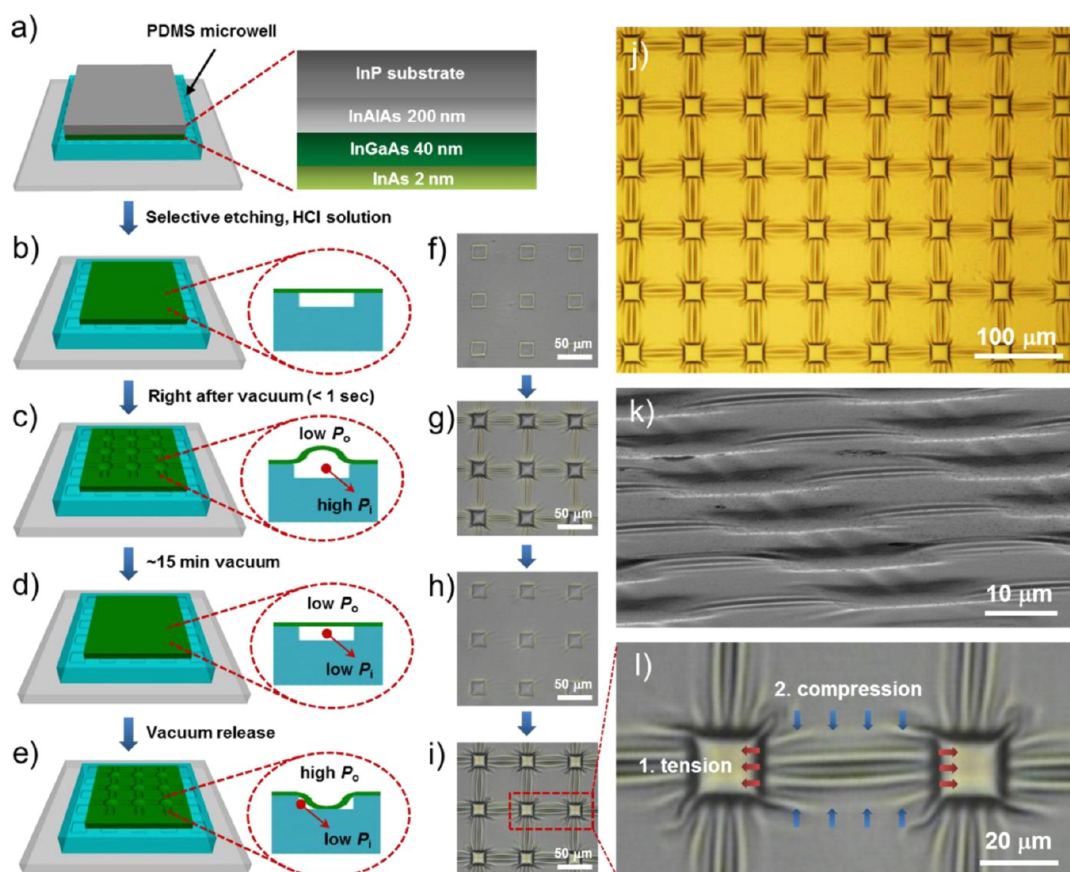


**Figure 1. (a−e) Schematic illustrations of the vacuum-induced wrinkling of III−V nanomembrane. (f−i) A series of optical microscope (OM) images of III−V nanomembranes during the vacuum-induced wrinkling process: (f) before the vacuum process, (g) right after the vacuum process, (h) ∼15 min after the vacuum process, and (i) right after the vacuum release. (j) Optical microscope image of nanomembrane wrinkle arrays formed between the microwell patterns after the vacuum process. (k) Tilt-view SEM image of wrinkled III−V nanomembrane. (l) Optical microscope image of the wrinkled III−V nanomembrane fabricated by the vacuum-induced longitudinal tension and the subsequent transverse compression.**

wrinkling process through use of various sizes and shapes of PDMS microwell patterns. When there is only one microwell pattern on the PDMS stamp, the compressive stress is localized near the fixed boundary of the microwell, resulting in the vague wrinkles near the edge of the pattern (Figure 2a). When the single microwell pattern is paired with another microwell pattern, the wrinkles created can extend over the entire region between the microwells, even for microwell patterns with larger longitudinal length (Figure 2b). For rectangular microwell patterns (50 × 10 $\mu m^2$), we observed wrinkle formation at high aspect ratio (longitudinal length to transverse width ratio, $L_1/W_1 = 10$) regions between the microwells, but observed either no or vague wrinkle formation at low aspect ratio ($L_2/W_2 = 1$) regions between the microwells (Figure 2c). This behavior agrees with the previous study reporting that larger critical strain is required for the onset of wrinkle formation in rectangular sheets with low aspect ratios.[40] For circular microwell patterns with hexagonal arrangement, we observed wrinkle formations with hexagonal arrangements between the circular microwells (Figure 2d).

While the formation and location of vacuum-induced wrinkles were induced by the tensile and compressive stress developed in between the microwell arrangements, the wavelength and amplitude of the wrinkles can be further engineered by varying the modulus of the underlying PDMS stamp, similar to traditional hard and soft bilayer structures.[28,41] Figure 3 shows optical and atomic force microscope (AFM) images of wrinkle arrays with different wavelengths and amplitudes controlled by the modulus of the underlying PDMS substrates. Initially, we observed that the wavelength of wrinkles decreases with an increase in the PDMS modulus. The AFM cross section analyses of wrinkles in the direction perpendicular to the applied tensile stress indicate a sinusoidal variation of amplitude, where the amplitude decays from the center toward the edge of the wrinkled domain of the nanomembrane between the microwells (Figure 3a−c). This damped sinusoidal deformation of wrinkles is different from the periodic sinusoidal deformation of wrinkles with singular wavelength and amplitude formed by the traditional mechanical stretching/releasing method.[10−12,14] The wrinkles with decaying amplitude observed in this

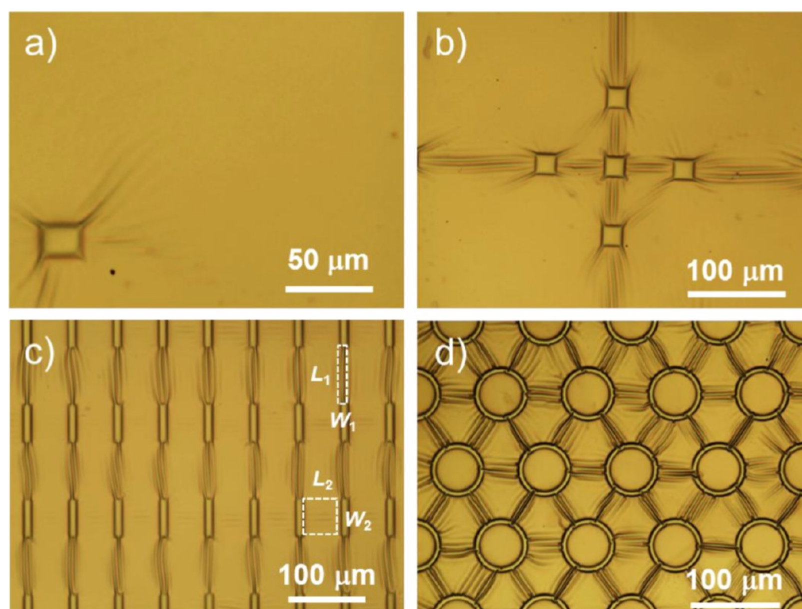


**Figure 2. Optical microscope images of nanomembrane wrinkles on (a) a single microwell, (b) paired microwells, (c) rectangular microwell arrays, and (d) circular microwell arrays.**

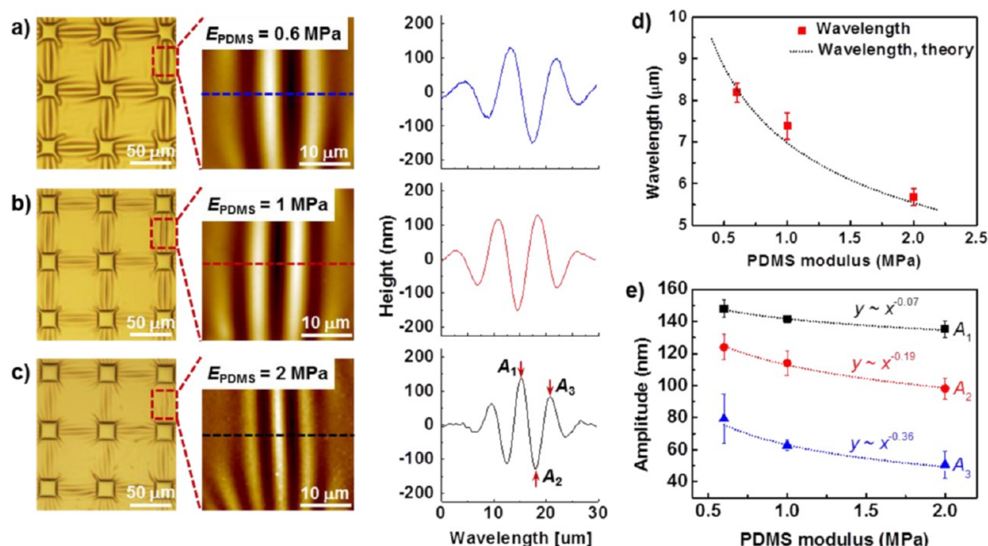


**Figure 3. (a−c) OM and atomic force microscope (AFM) images of nanomembrane wrinkles on PDMS microwell arrays at different PDMS modulus: (a) 0.6, (b) 1, and (c) 2 MPa. (d) The variation of wrinkle wavelength with different PDMS modulus. The dotted line is a theoretical fitting. (e) The variation of amplitudes for different values of PDMS modulus. The dotted lines are the power-law fitting to the experimental results.**

study can be attributed to the stretch-induced compressive stress profile, where the center area between the microwells is under the largest stress, resulting in the deepest amplitude of wrinkles.[37]

Detailed analysis of the wavelength variations as a function of PDMS modulus indicated that the wavelength decreased from ∼8.2 $\mu$m to ∼5.7 $\mu$m with an increase in PDMS modulus from 0.6 to 2.0 MPa (Figure 3d). To further understand the dependence of wavelength on the PDMS modulus, we compared the experimental results with theoretical calculations. Although the wrinkle deformation patterns (damped *vs* periodic sinusoidal wrinkles) are different, the dependence of wavelength on the PDMS modulus for the damped sinusoidal wrinkles can be described by the typical relation used for periodic sinusoidal wrinkles:[34,42]

$$\lambda = 2\pi h_f \left(\frac{\bar{E}_f}{3\bar{E}_s}\right)^{1/3} \qquad (1)$$

where $\lambda$ is the wavelength of wrinkle, $h_f$ and $\bar{E}_f$ are the height and plane-strain modulus of the upper film, and $\bar{E}_s$ is the plane-strain modulus of substrate. Here, the

plane-strain modulus can be represented by $\bar{E} = E/(1 - v^2)$, where $E$ and $v$ are Young's modulus and Poisson's ratio, respectively. The experimentally obtained wavelengths of the wrinkles fit well with the calculated wavelengths (eq 1) for InGaAs nanomembranes with $h_f = 42$ nm, $E_f = 65.8$ GPa,[43] and $v_f = 0.33$ as a function of PDMS modulus with $v_s = 0.5$ (Figure 3d), suggesting that eq 1 holds even for damped sinusoidal wrinkles.

The damped sinusoidal wrinkles showed a decaying amplitude profile, where the amplitude decayed from the center to the edge of the wrinkled domain, as marked with $A_1$, $A_2$, and $A_3$ in Figure 3c. The dependence of amplitude on the PDMS modulus is shown in Figure 3e, where the amplitude decreases with the PDMS modulus. A power law fitting to the experimental amplitudes resulted in exponents of −0.07, −0.19, and −0.36 for amplitudes of $A_1$, $A_2$, and $A_3$, respectively. This result indicates that the dependence of amplitude on the PDMS modulus increases from the center to the edge of the wrinkled domain. A power law dependence of amplitude on the substrate modulus is also observed for periodic sinusoidal wrinkles with single amplitude, where the amplitude can be expressed by[42]

$$A = h_f \sqrt{\frac{\varepsilon - \varepsilon_c}{\varepsilon_c}} \tag{2}$$

where $A$ is the amplitude of wrinkle, $\varepsilon$ and $\varepsilon_c$ are the strain and critical wrinkling strain, respectively, of the upper film. The critical wrinkling strain is given by:

$$\varepsilon_c = \frac{1}{4}\left(\frac{3\bar{E}_s}{\bar{E}_f}\right)^{2/3} \tag{3}$$

Equations 2 and 3 lead to a power law scaling of amplitude dependent on the substrate modulus ($E_s$) with power law exponent of −1/3 (*i.e.*, $A$ is proportional to $E_s^{-1/3}$), which is comparable to that of $A_3$ (−0.36).

Equation 2 also suggests that the amplitude of the wrinkle can be further controlled by the compressive strain ($\varepsilon$) of the nanomembranes. Here, we changed the depth of the microwell that determines the extent of inward bulging of the nanomembrane during the vacuum process and thus the longitudinal tensile strain, which, in turn, determines the compressive strain of nanomembranes. Figure 4a shows the wrinkle patterns fabricated by the vacuum-induced wrinkling process as a function of different depths ($d$) of the microwells. Detailed AFM cross section analysis (Figure 4b,c) indicated that the maximum amplitude ($A_1$) at the center of the damped sinusoidal profile increased from 68 to 175 nm when the microwell depth changed from 0.6 to 1.7 $\mu$m. This result indicates that the maximum amplitude ($A_1$) is strongly dependent on compressive strain while it is less dependent on the PDMS modulus. On the other hand, the wavelength does not change with the depth of the microwells, suggesting that the wavelength is

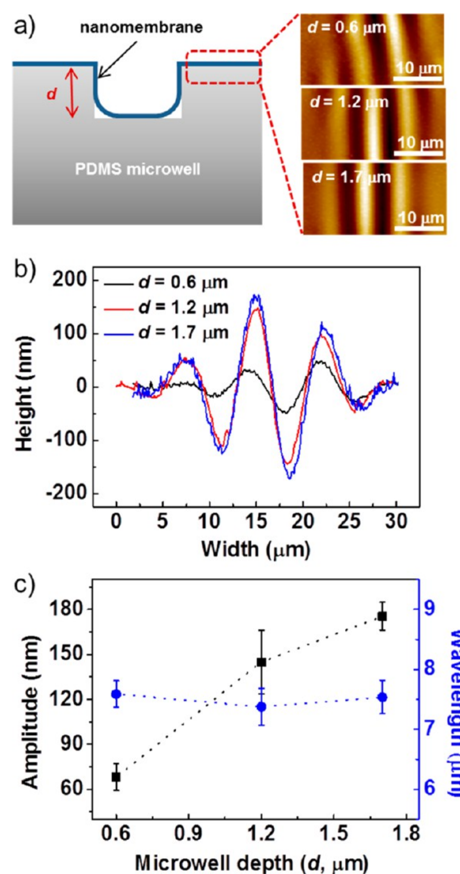


**Figure 4. (a) AFM images and (b) cross section analysis of nanomembrane wrinkles on different depth ($d$, 0.6, 1.2, 1.7 $\mu$m) of microwell patterns. (c) The variation of wavelength and amplitude of nanomembrane wrinkles with different depth of the microwell patterns.**

independent of compressive strain. Instead, as shown in Figure 3d, the wavelength is a function of PDMS modulus according to eq 1.[42]

The wavelength and amplitude of wrinkled nanomembranes can be further modulated during the transfer printing of nanomembranes onto the heterogeneous substrates. When the PDMS substrate temperature is varied during the transfer printing process, the thermal expansion or contraction of the PDMS stamp modifies the compressive strain of the nanomembranes, which leads to the modulation of the wavelength and amplitude of the nanomembrane wrinkles. Figure 5a shows a schematic illustration of the wrinkled nanomembrane transfer from the PDMS stamp onto the glass substrate coated with SU-8 photoresist. For the transfer printing at a laboratory temperature (∼25 °C), the original wavelength and amplitude of the nanomembrane wrinkles on the PDMS stamp were maintained after the transfer process (Figure 5c, Supporting Information Figure S3). When the temperature was decreased (10 °C) during the transfer process, the thermal contraction of the PDMS stamp further induced compressive strains on the nanomembranes, which led to growth of the

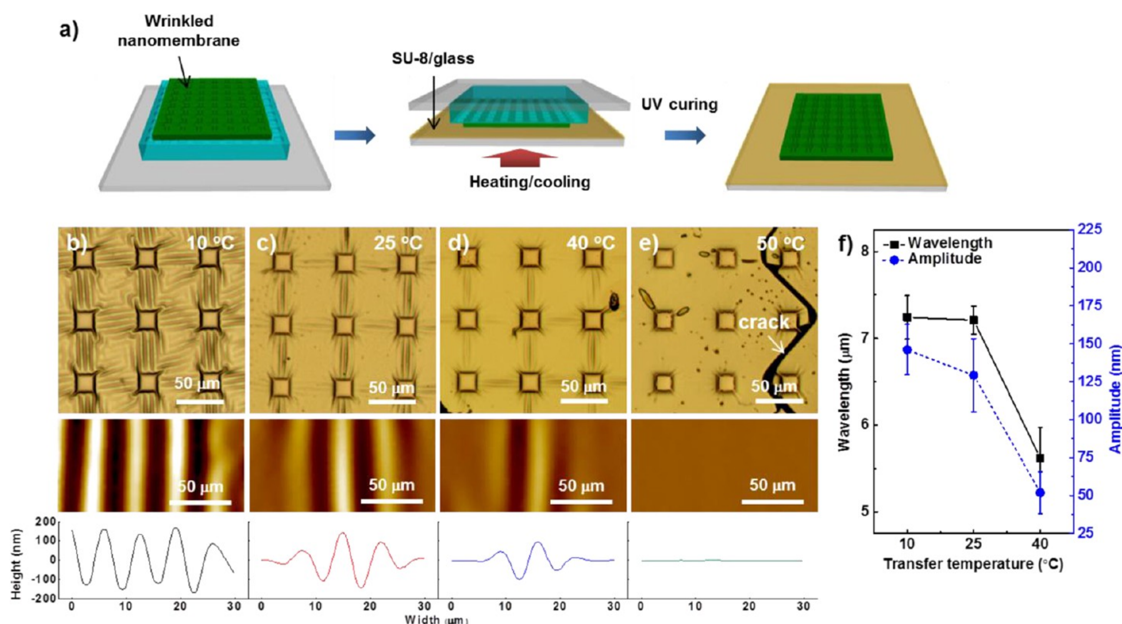


**Figure 5. (a) Schematic illustration of transfer printing of the wrinkled III−V nanomembrane from the PDMS to glass substrates. (b−e) OM images of the wrinkled III−V nanomembrane on SU-8/glass substrate after transfer printing at different temperatures: (b) 10, (c) 25, (d) 40, and (e) 50 °C. (f) The variation of wavelength and amplitude of nanomembrane wrinkles at different transfer printing temperatures.**

wrinkles (Figure 5b). Here, the amplitude of the wrinkles slightly increased from ~129 nm to ~146 nm while the wavelength did not change (Figure 5f). On the other hand, when the transfer temperature was increased to 40 °C, the wrinkles were stretched out due to thermal expansion of the PDMS, which led to the decrease of amplitude from ~129 to ~52 nm (Figure 5d,e). With further increase of transfer temperature to 50 °C, the original wrinkle patterns were flattened and disappeared, leading to a flat nanomembrane (Figure 5e). At this stage, we also observed the generation of cracks (indicated by a white arrow in Figure 5e) because the thermal expansion of the PDMS stamp was well over the critical thermal expansion of the nanomembranes.

## CONCLUSIONS

In summary, we demonstrated the formation of deterministic and multidirectional wrinkle arrays through vacuum-induced bulging of InGaAs nanomembranes on top of PDMS microwell arrays. Here, the local events of vacuum-induced stretching of nanomembranes under geometrical constraints of microwells enabled simple control of the direction and geometry of wrinkles through the shape, location, depth, and alignment of microwell arrays. The geometry of wrinkle arrays on PDMS substrates could be further engineered by controlling the transfer temperature during the transfer of wrinkled nanomembranes onto glass substrates. Since the carrier mobility and band structure of semiconductor nanomembranes changes with strain, the localized wrinkles controlled in microscopic length scales can be potentially used in locally tunable band gap engineering for strain-enhanced high mobility transistors,[44] light-emitting devices,[20] and single-element heterojunction superlattices.[25]

## MATERIALS AND METHODS

**Growth of III−V Semiconductor Films.** InAs/n-InGaAs/InAlAs stack layers were grown on InP substrates using a molecular beam epitaxy system (MBE, Riber Compact 21T). The *n*-InGaAs layer was doped by $3.05 \times 10^{18}$ $cm^3$ (at 440 °C). Both $In_{0.52}Al_{0.48}As$ and $In_{0.53}Ga_{0.47}As$ layers were completely lattice-matched to an InP (001) substrate. An $In_{0.53}Ga_{0.47}As$ buffer layer was used as an etch-stop layer, which was fundamental in the selective wet-etching process. The 2 nm InAs capping layer was used to prevent surface oxidation at atmosphere.

**Preparation of PDMS Stamp.** The microwell-patterned PDMS stamps were fabricated through a micromolding process with photoresist micropatterns (AZ5214E, Clariant Corp.) on Si substrates (Supporting Information Figure S1). The PDMS prepolymer was prepared by mixing different ratios of PDMS base to curing agent (10:1, 15:1, and 20:1) to control the Young's modulus of the PDMS. The mixed PDMS prepolymer was poured onto the micromold substrates, baked on top of a hot plate (4 h, 80 °C), and then peeled off from the micromolds. Here, the thickness of the PDMS stamp was controlled to be ~2 mm.

**Wrinkling Process.** The PDMS stamp and the compound semiconductor sample were rinsed with deionized (DI) water and isopropyl alcohol (IPA), and dried by blowing nitrogen gas. The upper layers (InAs/n-InGaAs) of the III−V multilayer substrate were attached to the patterned side of the PDMS stamp by conformal contacts. The attached III−V substrate was then etched in an HCl solution (37% HCl, $HCl/H_2O$ = 2.3:1 volume ratio) containing 0.058 wt % of surfactant (sodium dodecyl sulfate, SDS) at 40 °C for 30 min. The SDS surfactant was used to

prevent bubble formation on the etched surfaces during the wet-etching process. After the wet-etching process, the nanomembranes consisting of 40 nm InGaAs layer capped with a 2 nm InAs layer on PDMS stamps were carefully rinsed with DI water and blown dry using nitrogen gas. Then, the samples were put into a small chamber connected to a regular mechanical pump. Finally, the evacuation process (~65 kPa) for 15 min and the subsequent releasing of vacuum resulted in the formation of nanomembrane wrinkle arrays on top of PDMS microwell arrays.

**Transfer Printing of Wrinkled Nanomembranes.** A glass substrate was rinsed by sonication in IPA and coated with SU-8 50 (MicroChem Corp.) by spin-coating (4000 rpm, 3 min). The PDMS stamp with the wrinkled nanomembrane was attached to the glass substrate coated with a precured SU-8 layer and completely dried for ~2 days at different temperatures (10−50 °C). Finally, SU-8 was cured by UV exposure for 10 min and the PDMS stamp was peeled off from the SU-8/glass substrate, resulting in the transfer of the wrinkled nanomembrane onto the glass substrate.

**Characterizations.** Atomic force microscopy (AFM, Dimension, Veeco) was used to characterize the surface wrinkles of the nanomembranes. The SEM images of wrinkled nanomembranes were obtained using field-emission scanning electron microscopy (SEM, S-4800, Hitachi). A universal testing machine (WL2100, Withlab Corp.) was used to for measuring the PDMS Young's modulus (Supporting Information Figure S4). The test speed was 5 mm/min at 23 °C and 50% relative humidity.

*Conflict of Interest:* The authors declare no competing financial interest.

*Acknowledgment.* This work was supported by the National Research Foundation of Korea (NRF-2011-0014965, NRF-2012K1A3A1A20031618), BK21 Plus Program (10Z20130011057), and KIST Institutional Program.

*Supporting Information Available:* Cross-sectional TEM image of the epitaxially grown multilayers, additional SEM images of wrinkled nanomembranes, Young's modulus of PDMS films, and videos of wrinkle formation are included. This material is available free of charge *via* the Internet at http://pubs.acs.org.

## REFERENCES AND NOTES


1. Rogers, J. A.; Lagally, M. G.; Nuzzo, R. G. Synthesis, Assembly and Applications of Semiconductor Nanomembranes. *Nature* **2011**, *477*, 45–53.
2. Ko, H.; Takei, K.; Kapadia, R.; Chuang, S.; Fang, H.; Leu, P. W.; Ganapathi, K.; Plis, E.; Kim, H. S.; Chen, S. Y.; *et al.* Ultrathin Compound Semiconductor on Insulator Layers for High-Performance Nanoscale Transistors. *Nature* **2010**, *468*, 286–289.
3. Fang, H.; Chuang, S.; Takei, K.; Kim, H. S.; Plis, E.; Liu, C.-H.; Krishna, S.; Chueh, Y.-L.; Javey, A. Ultrathin-Body High-Mobility InAsSb-on-Insulator Field-Effect Transistors. IEEE. *Electron Device Lett.* **2012**, *33*, 504–506.
4. Wang, C.; Chien, J. C.; Fang, H.; Takei, K.; Nah, J.; Plis, E.; Krishna, S.; Niknejad, A. M.; Javey, A. Self-Aligned, Extremely High Frequency III-V Metal-Oxide-Semiconductor Field-Effect Transistors on Rigid and Flexible Substrates. *Nano Lett.* **2012**, *12*, 4140–4145.
5. Ahn, J. H.; Kim, H. S.; Lee, K. J.; Jeon, S.; Kang, S. J.; Sun, Y.; Nuzzo, R. G.; Rogers, J. A. Heterogeneous Three-Dimensional Electronics by Use of Printed Semiconductor Nanomaterials. *Science* **2006**, *314*, 1754–1757.
6. Nah, J.; Fang, H.; Wang, C.; Takei, K.; Lee, M. H.; Plis, E.; Krishna, S.; Javey, A. III-V Complementary Metal-Oxide-Semiconductor Electronics on Silicon Substrates. *Nano Lett.* **2012**, *12*, 3592–3595.
7. Yoon, J.; Jo, S.; Chun, I. S.; Jung, I.; Kim, H. S.; Meitl, M.; Menard, E.; Li, X.; Coleman, J. J.; Paik, U.; *et al.* GaAs Photovoltaics and Optoelectronics Using Releasable Multilayer Epitaxial Assemblies. *Nature* **2010**, *465*, 329–333.
8. Park, S. I.; Xiong, Y.; Kim, R. H.; Elvikis, P.; Meitl, M.; Kim, D. H.; Wu, J.; Yoon, J.; Yu, C. J.; Liu, Z.; *et al.* Printed Assemblies of Inorganic Light-Emitting Diodes for Deformable and Semitransparent Displays. *Science* **2009**, *325*, 977–981.
9. Kim, R.-H.; Kim, D.-H.; Xiao, J.; Kim, B. H.; Park, S.-I.; Panilaitis, B.; Ghaffari, R.; Yao, J.; Li, M.; Liu, Z.; *et al.* Waterproof AlInGaP optoelectronics on stretchable substrates with applications in biomedicine and robotics. *Nat. Mater.* **2010**, *9*, 929–937.
10. Khang, D. Y.; Jiang, H.; Huang, Y.; Rogers, J. A. A Stretchable Form of Single-Crystal Silicon for High-Performance Electronics on Rubber Substrates. *Science* **2006**, *311*, 208–212.
11. Sun, Y.; Kumar, V.; Adesida, I.; Rogers, J. A. Buckled and Wavy Ribbons of GaAs for High-Performance Electronics on Elastomeric Substrates. *Adv. Mater.* **2006**, *18*, 2857–2862.
12. Sun, Y.; Choi, W. M.; Jiang, H.; Huang, Y. Y.; Rogers, J. A. Controlled Buckling of Semiconductor Nanoribbons for Stretchable Electronics. *Nat. Nanotechnol.* **2006**, *1*, 201–207.
13. Rogers, J. A.; Someya, T.; Huang, Y. Materials and Mechanics for Stretchable Electronics. *Science* **2010**, *327*, 1603–1607.
14. Jiang, H.; Khang, D. Y.; Song, J.; Sun, Y.; Huang, Y.; Rogers, J. A. Finite Deformation Mechanics in Buckled Thin Films on Compliant Supports. *Proc. Natl. Acad. Sci. U. S. A.* **2007**, *104*, 15607–15612.
15. Koo, W. H.; Jeong, S. M.; Araoka, F.; Ishikawa, K.; Nishimura, S.; Toyooka, T.; Takezoe, H. Light Extraction from Organic Light-Emitting Diodes Enhanced by Spontaneously Formed Buckles. *Nat. Photonics* **2010**, *4*, 222–226.
16. Lipomi, D. J.; Tee, B. C.; Vosgueritchian, M.; Bao, Z. Stretchable Organic Solar Cells. *Adv. Mater.* **2011**, *23*, 1771–1775.
17. Kim, J. B.; Kim, P.; Pégard, N. C.; Oh, S. J.; Kagan, C. R.; Fleischer, J. W.; Stone, H. A.; Loo, Y.-L. Wrinkles and Deep Folds as Photonic Structures in Photovoltaics. *Nat. Photonics* **2012**, *6*, 327–332.
18. Mei, Y.; Kiravittaya, S.; Benyoucef, M.; Thurmer, D. J.; Zander, T.; Deneke, C.; Cavallo, F.; Rastelli, A.; Schmidt, O. G. Optical Properties of a Wrinkled Nanomembrane with Embedded Quantum Well. *Nano Lett.* **2007**, *7*, 1676–1679.
19. Jain, J. R.; Hryciw, A.; Baer, T. M.; Miller, D. A.; Brongersma, M. L.; Howe, R. T. A Micromachining-Based Technology for Enhancing Germanium Light Emission *via* Tensile Strain. *Nat. Photonics* **2012**, *6*, 398–405.
20. Roberts, M. M.; Klein, L. J.; Savage, D. E.; Slinker, K. A.; Friesen, M.; Celler, G.; Eriksson, M. A.; Lagally, M. G. Elastically Relaxed Free-Standing Strained-Silicon Nanomembranes. *Nat. Mater.* **2006**, *5*, 388–393.
21. Feng, J.; Qian, X.; Huang, C.-W.; Li, J. Strain-Engineered Artificial Atom as a Broad-Spectrum Solar Energy Funnel. *Nat. Photonics* **2012**, *6*, 866–872.
22. Asai, H.; Oe, K. Energy Band-Gap Shift with Elastic Strain in $Ga_xIn_{1-x}P$ Epitaxial Layers on (001) GaAs Substrates. *J. Appl. Phys.* **1983**, *54*, 2052–2056.
23. Signorello, G.; Karg, S.; Bjork, M. T.; Gotsmann, B.; Riel, H. Tuning the Light Emission from GaAs Nanowires over 290 meV with Uniaxial Strain. *Nano Lett.* **2013**, *13*, 917–924.
24. Huang, M.; Ritz, C. S.; Novakovic, B.; Yu, D.; Zhang, Y.; Flack, F.; Savage, D. E.; Evans, P. G.; Knezevic, I.; Liu, F. Mechano-electronic Superlattices in Silicon Nanoribbons. *ACS Nano* **2009**, *3*, 721–727.
25. Liu, Z.; Wu, J.; Duan, W.; Lagally, M. G.; Liu, F. Electronic Phase Diagram of Single-Element Silicon "Strain" Superlattices. *Phys. Rev. Lett.* **2010**, *105*, 016802.
26. Hon, N. K.; Tsia, K. K.; Solli, D. R.; Jalali, B. Periodically Poled Silicon. *Appl. Phys. Lett.* **2009**, *94*, 091116.
27. Lin, Y.-M.; Dresselhaus, M. S. Thermoelectric Properties of Superlattice Nanowires. *Phys. Rev. B* **2003**, *68*, 075304.
28. Bowden, N.; Brittain, S.; Evans, A. G.; Hutchinson, J. W.; Whitesides, G. M. Spontaneous Formation of Ordered Structures in Thin Films of Metals Supported on an Elastomeric Polymer. *Nature* **1998**, *393*, 146–149.
29. Huck, W. T.; Bowden, N.; Onck, P.; Pardoen, T.; Hutchinson, J. W.; Whitesides, G. M. Ordering of Spontaneously Formed Buckles on Planar Surfaces. *Langmuir* **2000**, *16*, 3497–3501.

30. Vandeparre, H.; Desbief, S.; Lazzaroni, R.; Gay, C.; Damman, P. Confined Wrinkling: Impact on Pattern Morphology and Periodicity. *Soft Matter* **2011**, *7*, 6878–6882.
31. Vandeparre, H.; Damman, P. Wrinkling of Stimuloresponsive Surfaces: Mechanical Instability Coupled to Diffusion. *Phys. Rev. Lett.* **2008**, *101*, 124301.
32. Chan, E. P.; Crosby, A. J. Fabricating Microlens Arrays by Surface Wrinkling. *Adv. Mater.* **2006**, *18*, 3238–3242.
33. Chung, J. Y.; Nolte, A. J.; Stafford, C. M. Diffusion-Controlled, Self-Organized Growth of Symmetric Wrinkling Patterns. *Adv. Mater.* **2009**, *21*, 1358–1362.
34. Stafford, C. M.; Harrison, C.; Beers, K. L.; Karim, A.; Amis, E. J.; VanLandingham, M. R.; Kim, H. C.; Volksen, W.; Miller, R. D.; Simonyi, E. E. A Buckling-Based Metrology for Measuring the Elastic Moduli of Polymeric Thin Films. *Nat. Mater.* **2004**, *3*, 545–550.
35. Efimenko, K.; Rackaitis, M.; Manias, E.; Vaziri, A.; Mahadevan, L.; Genzer, J. Nested Self-Similar Wrinkling Patterns in Skins. *Nat. Mater.* **2005**, *4*, 293–297.
36. Yin, J.; Yague, J. L.; Eggenspieler, D.; Gleason, K. K.; Boyce, M. C. Deterministic Order in Surface Micro-Topologies through Sequential Wrinkling. *Adv. Mater.* **2012**, *24*, 5441–5446.
37. Nayyar, V.; Ravi-Chandar, K.; Huang, R. Stretch-Induced Stress Patterns and Wrinkles in Hyperelastic Thin Sheets. *Int. J. Solids Struct.* **2011**, *48*, 3471–3483.
38. Cerda, E.; Ravi-Chandar, K.; Mahadevan, L. Wrinkling of an Elastic Sheet under Tension. *Nature* **2002**, *419*, 579–580.
39. Cerda, E.; Mahadevan, L. Geometry and Physics of Wrinkling. *Phys. Rev. Lett.* **2003**, *90*, 074302.
40. Kim, T.-Y.; Puntel, E.; Fried, E. Numerical Study of the Wrinkling of a Stretched Thin Sheet. *Int. J. Solids Struct.* **2012**, *49*, 771–782.
41. Armani, D.; Liu, C.; Aluru, N. Re-configurable Fluid Circuits by PDMS Elastomer Micromachining. In *Micro Electro Mechanical Systems, 1999. MEMS'99. Twelfth IEEE International Conference on*, Orlando, FL, January, 1999; IEEE: Piscataway, NJ, 1999; pp 222−227.
42. Chung, J. Y.; Nolte, A. J.; Stafford, C. M. Surface Wrinkling: A Versatile Platform for Measuring Thin-Film Properties. *Adv. Mater.* **2011**, *23*, 349–368.
43. Detz, H.; Strasser, G. Modeling the Elastic Properties of the Ternary III-V Alloys InGaAs, InAlAs and GaAsSb Using Tersoff Potentials for Binary Compounds. *Semicond. Sci. Technol.* **2013**, *28*, 085011.
44. Chu, M.; Sun, Y.; Aghoram, U.; Thompson, S. E. Strain: A Solution for Higher Carrier Mobility in Nanoscale MOSFETs. *Ann. Rev. Mater. Res.* **2009**, *39*, 203–229.